An eddy-viscosity model for turbulent flows of Herschel–Bulkley fluids

Lovato, S.; Keetels, G. H.; Toxopeus, S. L.; Settels, J. W.

DOI
10.1016/j.jnnfm.2021.104729

Publication date
2022

Document Version
Final published version

Published in
Journal of Non-Newtonian Fluid Mechanics

Journal of Non-Newtonian Fluid Mechanics 301 (2022) 104729

Contents lists available at ScienceDirect

Journal of Non-Newtonian Fluid Mechanics

journal homepage: www.elsevier.com/locate/jnnfm

An eddy-viscosity model for turbulent flows of Herschel–Bulkley fluids

S. Lovato [a,*], G.H. Keetels [a], S.L. Toxopeus [b], J.W. Settels [b]

[a] Delft University of Technology, P.O. Box 5, Delft 2600AA, The Netherlands
[b] Maritime Research Institute Netherlands, P.O. Box 28, Wageningen 6700AA, The Netherlands

ARTICLE INFO

Keywords:
Yield stress
Shear-thinning
RANS
Pipe flow
Non-Newtonian
CFD

ABSTRACT

This article presents a new turbulence closure based on the k-ω SST model for predicting turbulent flows of Herschel–Bulkley fluids, including Bingham and power-law fluids. The model has been calibrated with direct numerical simulations (DNS) data for fully-developed pipe flow of shear-thinning and viscoplastic fluids. The new model shows good agreement in the mean velocity, average viscosity, mean shear stress budget and friction factor. The latter compares well also against correlations from the literature for a wide range of Reynolds numbers. With the new model, improvements are also observed in the iterative convergence, which is often difficult for calculations with yield-stress fluids. Additionally, three eddy-viscosity models for Newtonian fluids, namely the k-ω SST, k-$\sqrt{k}L$ and Spalart–Allmaras model, have been tested on turbulent Herschel–Bulkley flows. Results show that (i) the new model produces the best prediction; (ii) the standard SST model may be considered for simulations of weakly shear-thinning/viscoplastic fluids at high Reynolds numbers; (iii) the k-$\sqrt{k}L$ and the Spalart–Allmaras models appear to be unsuitable for turbulent Herschel–Bulkley flows. The new model is simple and appealing for engineering applications concerned with turbulent wall-bounded flows and is presented in a formulation that can be easily adapted to other generalised Newtonian fluids.

1. Introduction

Numerical simulations of turbulent Herschel–Bulkley flows are of great interest for several industrial applications, such as open channel flows of ore tailings in the mining industry or pipe flows of drilling mud in the oil industry. Recently, numerical studies of turbulent Herschel–Bulkley flows have become of interest even for the maritime sector, with regard to the effects of muddy seabeds on marine vessels navigating in harbours and rivers [1,2].

The prohibitive costs of Direct Numerical Simulations (DNS) for predicting turbulent flows makes turbulence modelling the only feasible alternative for most engineering applications as it offers an acceptable compromise between cost and accuracy. The most widespread modelling technique is the so-called Reynolds-averaging, which makes use of the Reynolds-averaged Navier–Stokes (RANS) equations. These models are therefore usually referred to as RANS models.

For Newtonian fluids, several RANS models are typically available in general-purpose Computational Fluid Dynamics (CFD) codes. On the other hand, RANS models for Herschel–Bulkley fluids have not yet received enough recognition in the CFD community, thus CFD practitioners often apply Newtonian RANS models to non-Newtonian fluids, and this continued to happen until very recently (e.g., [1–5]).

The two main difficulties concerning the Reynolds-averaged modelling for non-Newtonian fluids are the shear-dependent viscosity and the appearance of extra correlations in the governing equations as a result of the fluctuating viscosity. These correlations are unknown *a priori* and therefore require a closure.

Significant progress has been made for viscoelastic fluids in the past twenty years. Pinho [6] derived a low Reynolds number formulation based on the k-ϵ model of Nagano and Hishida [7]. The formulation included both a turbulence closure for some of the non-Newtonian correlations and a model for the average viscosity that accounted for fluctuations of the shear and strain rate. The model showed reasonable agreement with experimental data [8] and it laid the foundation for later advance in turbulence modelling for non-Newtonian fluids. The model was improved [9] to include the cross-correlation between the fluctuating viscosity and the fluctuating deformation rate tensor. Subsequently, the model was extended to finitely extensible-nonlinear-elastic fluids with Peterlin's approximation (FENE-P) [10] and finally improved [11] for better prediction at a higher level of drag reduction, also using a k-ω type closure [12].

One limitation of two-equation models is that they assume isotropic turbulence. While this assumption is generally acceptable for Newtonian fluids, it is now known that the turbulence for non-Newtonian fluids exhibits higher level of anisotropy (e.g. [13,14]). Iaccarino et al. [15] developed a closure for FENE-P fluids based on the k-ϵ-$v2$-f model

* Corresponding author.
E-mail address: s.l.lovato@tudelft.nl (S. Lovato).

https://doi.org/10.1016/j.jnnfm.2021.104729
Received 5 July 2021; Received in revised form 30 November 2021; Accepted 16 December 2021
Available online 10 January 2022

of Durbin [16], which is able to reproduce the inviscid wall-blocking of cross-stream velocity fluctuations without the need of damping functions. An improved version was proposed by Masoudian et al. [17], which extended the validity of the model of Iaccarino et al. [15] up to the maximum drag reduction. Masoudian et al. [18] proposed a closure for FENE-P fluids also based on the Reynolds-stress model (RSM).

Fewer studies have dealt with inelastic fluids such as power-law, Bingham and Herschel–Bulkley. Firsts efforts date back to 1997, when Malin [19,20] modified the damping function in the eddy viscosity of the k-ϵ model of Lam and Bremhorst [21]. The modification accounted for the shear-thinning rheology and results showed fairly good agreement against experimental data on the friction factor and mean velocity profile of pipe flows. However, apart from the modified damping function, results were obtained with a Newtonian RANS model, hence no turbulence closure was used for the non-Newtonian correlations. A similar approach was adopted by Bartosik [22,23], who modified the damping function of the k-ϵ model accounting for the yield stress of Bingham and Herschel–Bulkley fluids. Recently, a significant step forward has been made by Gavrilov and Rudyak [24], who proposed a turbulence closure for power-law fluids, using the k-ϵ-$v2$-f model of Durbin [16].

This work aims at developing a RANS model for Herschel–Bulkley fluids that introduces the minimum amount of complexities while capturing the relevant physics of interest for engineering applications concerned with wall-bounded flows. In this article the turbulent closure of Gavrilov and Rudyak [24] for power-law fluids is extended to Herschel–Bulkley fluids and is presented in a general form that can be easily extended to any generalised Newtonian (GN) fluid model. However, instead of using the k-ϵ-$v2$-f model, the new model is developed starting from the popular k-ω SST model of Menter et al. [25]. The latter was developed for Newtonian fluids and it was proved to be a robust and accurate model for a large number of applications, including wall-bounded flows with adverse pressure gradient, which makes it suitable for turbulent flows of Newtonian fluids around bluff bodies. Being a blending of the k-ϵ [26] and k-ω [27] models, the SST model inherits their best features, i.e. the insensitivity to free-stream parameters of the k-ϵ and the accuracy in the near-wall region of the k-ω without using damping functions.

The results obtained with the new model are compared against recent DNS of Singh et al. [14,28,29] for fully-developed pipe flow and against correlations for the friction factor, covering a wide range of rheological parameters and Reynolds numbers.

An additional contribution of this work is the assessment of three Newtonian RANS models when they are applied to turbulent flows of Herschel–Bulkley fluids. The selected RANS models are: the $k-\omega$ SST [25], the $k-\sqrt{k}L$ [30] and the Spalart–Allmaras [31] models.

The rest of the paper is structured as follows. Section 2 describes the governing equations and the Reynolds-averaged procedure. The mathematical derivation of the turbulence closure is given in Section 3. An overview of the flow solver used in the present work is given in Section 5. Section 6 discusses numerical errors. Results are reported and discussed in Section 7. Finally, Section 8 summarises the main conclusions.

2. Governing equations

The incompressible flow is governed by the following continuity and momentum equations (the hat symbol denotes instantaneous quantities):

$$\nabla \cdot \hat{\boldsymbol{u}} = 0\,, \tag{1}$$

$$\frac{\partial(\rho\hat{\boldsymbol{u}})}{\partial t} + \nabla\cdot(\rho\hat{\boldsymbol{u}}\,\hat{\boldsymbol{u}}) = \nabla\cdot\hat{\boldsymbol{\tau}} - \nabla\hat{p}\,, \tag{2}$$

where $\hat{\boldsymbol{u}}(\boldsymbol{x},t)$ is the velocity vector, $\boldsymbol{x}$ is the position vector, t is time, $\hat{p}$ is pressure, ρ is density, $\hat{\boldsymbol{\tau}}$ is the deviatoric stress tensor that, for GN fluids, reads

$$\hat{\boldsymbol{\tau}} \equiv \hat{\tau}_{ij} = 2\hat{\mu}\hat{\boldsymbol{S}}\,, \qquad \hat{\boldsymbol{S}} \equiv \hat{S}_{ij} = \frac{1}{2}\left(\frac{\partial\hat{u}_i}{\partial x_j} + \frac{\partial\hat{u}_j}{\partial x_i}\right), \tag{3}$$

where $\hat{S}_{ij}$ is the deformation rate tensor and $\hat{\mu}$ is the apparent viscosity. For Newtonian fluids, the apparent viscosity is simply a constant equal to the molecular viscosity, whereas for GN fluids the apparent viscosity is a function of the instantaneous shear rate $\dot{\hat{\gamma}} = \sqrt{2\hat{S}_{ij}\hat{S}_{ij}}$. In particular, for Herschel–Bulkley fluids, the apparent viscosity reads (e.g. [32])

$$\begin{cases} \hat{\mu} = \dfrac{\tau_0 + K\,\dot{\hat{\gamma}}^n}{\dot{\hat{\gamma}}}\,, & \tau_0 \le |\hat{\boldsymbol{\tau}}|\,, \\ \hat{\mu} = \infty\,, & |\hat{\boldsymbol{\tau}}| < \tau_0\,, \end{cases} \tag{4}$$

where τ_0 is the yield stress, $|\hat{\boldsymbol{\tau}}| = \sqrt{\hat{\tau}_{ij}\hat{\tau}_{ij}/2}$ is the second invariant of $\hat{\tau}_{ij}$, n is the flow index and K is the consistency parameter, which has dimension of a viscosity for $n = 1$. The infinite viscosity in Eq. (4) means that the fluid does not deform ($\hat{\boldsymbol{S}} = 0$) when the stress level is below the yield stress. The Herschel–Bulkley model reduces to Bingham or power-law when $n = 1$ or $\tau_0 = 0$, respectively.

To avoid numerical difficulties associated with the infinite viscosity, the popular regularisation approach of Papanastasiou [33] is used. Thus, the apparent viscosity for the Herschel–Bulkley model given by Eq. (4) is replaced by

$$\hat{\mu} = \frac{\tau_0(1 - e^{-m\dot{\hat{\gamma}}}) + K\,\dot{\hat{\gamma}}^n}{\dot{\hat{\gamma}}}\,, \tag{5}$$

where m is the regularisation parameter. In the limit of $m \to \infty$, Eq. (5) tends to Eq. (4).

2.1. Reynolds-averaged equations

Following the procedure originally proposed by Osborne Reynolds (1895), a generic instantaneous flow quantity $\hat{\phi}$ can be expressed as the sum of a mean and a fluctuating part (Reynolds decomposition),

$$\hat{\phi}(\boldsymbol{x},t) = \phi(\boldsymbol{x},t) + \phi'(\boldsymbol{x},t)\,. \tag{6}$$

The mean value, $\phi(\boldsymbol{x},t)$, is here obtained from ensemble-averaging,[1] hence

$$\phi(\boldsymbol{x},t) = \overline{\hat{\phi}}(\boldsymbol{x},t) \equiv \frac{1}{N}\lim_{N\to\infty}\sum_{n=1}^{N}\hat{\phi}_n(\boldsymbol{x},t)\,, \tag{7}$$

with N being the number of repeated observations of $\hat{\phi}_n(\boldsymbol{x},t)$. This operation is known as Reynolds-averaging and it will be indicated with the overbar.

By applying the Reynolds-averaging to Eqs. (1) and (2), the Reynolds-averaged continuity and momentum equations for GN fluids are obtained:

$$\nabla\cdot\boldsymbol{u} = 0\,, \tag{8}$$

$$\rho\frac{\partial\boldsymbol{u}}{\partial t} + \rho\nabla\cdot(\boldsymbol{u}\,\boldsymbol{u}) = \nabla\cdot\tau - \nabla p - \rho\nabla\cdot(\overline{\boldsymbol{u}'\,\boldsymbol{u}'}) + \nabla\cdot\tau_{ij}^{nn}\,, \tag{9}$$

where $-\rho\overline{\boldsymbol{u}'\,\boldsymbol{u}'}$ is the (unknown) Reynolds stress tensor and $\tau \equiv \tau_{ij} = 2\mu S_{ij}$ is the mean deviatoric stress tensor. As a result of the fluctuating viscosity for non-Newtonian fluids, an additional term appears on the right-hand side of Eq. (9),

$$\tau_{ij}^{nn} = 2\overline{\mu' S'_{ij}}\,. \tag{10}$$

This term, hereafter referred to as non-Newtonian stress tensor, is *a priori* unknown and it requires turbulent closure.

[1] Contrary to $\phi'(\boldsymbol{x},t)$, the time dependency of $\phi(\boldsymbol{x},t)$ is relative to the nonturbulent unsteadiness of the flow.

2.2. Turbulence modelling

The turbulence model proposed in this article is based on the two-equation k-ω SST model of Menter et al. [25], which approximates the Reynolds stress tensor using the Boussinesq hypothesis,

$$-\rho\overline{u_i'u_j'} = \mu_t S_{ij} - \frac{2}{3}\rho\delta_{ij}k \tag{11}$$

where δ_{ij} is the Kronecker symbol, $k = \frac{1}{2}\overline{u_i'u_i'}$ is the turbulent kinetic energy (TKE) and μ_t is the so-called eddy (or turbulent) viscosity. The eddy viscosity is a function of k and ω, the latter being the specific dissipation rate of TKE. The variation of k and ω in the flow is modelled by two respective transport equations.

The transport equation for the turbulent kinetic energy k can be derived from the transport equations of the Reynolds stress by summation over the diagonal components (see e.g. [34] for the complete derivation), and it has the following expression:

$$\frac{D(\rho k)}{Dt} = P + \Pi + T + \mathscr{D} - \rho\epsilon + \xi^{nn} + \chi^{nn} + \mathscr{D}^{nn}\,. \tag{12}$$

The first four terms on the right-hand side are:

- production: $P = -\rho\overline{u_i'u_j'}S_{ij}$
- pressure diffusion: $\Pi = -\dfrac{\partial\overline{p'u_j'}}{\partial x_j}$
- turbulent transport: $T = -\dfrac{\partial\overline{\rho u_i'u_i'u_j'}}{\partial x_j}$
- mean viscous transport: $\mathscr{D} = \dfrac{\partial}{\partial x_j}\left(\mu\dfrac{\partial k}{\partial x_j} + \mu\dfrac{\partial\overline{u_i'u_j'}}{\partial x_i}\right)$
- viscous dissipation: $\rho\epsilon = 2\mu\overline{S_{ij}'S_{ij}'} + 2\overline{\mu' S_{ij}'S_{ij}'}$

The above terms are the same that are found in the equation for Newtonian fluids except for ϵ, that now contains the non-Newtonian contribution due to the fluctuating viscosity. The last three terms in Eq. (12) are non-Newtonian contributions and, adopting the terminology of Singh et al. [28], they read:

- mean shear turbulent viscous dissipation: $\chi^{nn} = -2\overline{\mu' S_{ij}'}S_{ij}$
- mean shear turbulent viscous transport: $\xi^{nn} = \dfrac{\partial(2\overline{\mu' u_i'}S_{ij})}{\partial x_j}$
- turbulent viscous transport: $\mathscr{D}^{nn} = \dfrac{\partial}{\partial x_j}\left(\frac{1}{2}\overline{\mu'\dfrac{\partial u_i'u_i'}{\partial x_j}} + \overline{\mu'\dfrac{\partial u_i'u_j'}{\partial x_i}}\right)$

Note that all the non-Newtonian contributions contain the fluctuating viscosity μ', therefore they all vanish when the fluid is Newtonian.

The first five terms of Eq. (12) are modelled as in the standard $k-\omega$ SST model (which is reported in Appendix A), hence:

$$\frac{D(\rho k)}{Dt} = \overbrace{\tilde{P}_k}^{P} + \overbrace{\nabla\cdot\left[(\mu+\sigma_k\mu_t)\nabla k\right]}^{\mathscr{D}+\Pi+T} - \rho\overbrace{\beta^* k\omega}^{\epsilon} + \xi^{nn} + \chi^{nn} + \mathscr{D}^{nn}\,. \tag{13}$$

$$\tilde{P}_k = \min(\mu_t S^2, 10\beta^*\rho k\omega)$$

where $S^2 = 2S_{ij}S_{ij}$. Eq. (13) is thus equal to the equation of the $k-\omega$ SST model except for the shear-dependent viscosity μ and the non-Newtonian contributions on the right-hand side that need to be modelled.

The exact transport equation of ω for GN fluids is lengthy and it can be derived from the exact transport equation of ϵ in [34]. Following the approach of Gavrilov and Rudyak [24], in the present work we consider the same empirical equation of the $k-\omega$ SST model, except for an additional (not yet specified) non-Newtonian contribution (E^{nn}):

$$\frac{D(\rho\omega)}{Dt} = \rho\alpha S^2 + \nabla\cdot\left[(\mu+\sigma_\omega\mu_t)\nabla\omega\right] - \beta\rho\omega^2 + 2\rho(1-F_1)\frac{\sigma_{\omega 2}}{\omega}\nabla k\cdot\nabla\omega + E^{nn}\,. \tag{14}$$

In order to solve Eqs. (9), (13) and (14), the unknown non-Newtonian contributions τ_{ij}^{nn}, ξ^{nn}, χ^{nn}, $\mathscr{D}^{nn}$, ϵ^{nn} and E^{nn} require turbulent closure. This is the topic of the next section.

3. Turbulence closure for the non-Newtonian terms

The closure is derived along the lines of Gavrilov and Rudyak [24]. The main difference is that in this work the closure is derived for the k-ω SST model and in a general form that can be easily extended to any GN model.

3.1. Average viscosity model

The average viscosity model proposed in [24] assumes that the average viscosity is a function of the mean shear rate, i.e

$$\overline{\hat{\mu}(\hat{\dot{\gamma}})} \simeq \mu(\bar{\dot{\gamma}}) \equiv \mu(\dot{\gamma})\,. \tag{15}$$

In turn, the mean shear rate (squared) reads:

$$\dot{\gamma}^2 = \overline{2\hat{S}_{ij}\hat{S}_{ij}} = 2S_{ij}S_{ij} + 2\overline{S_{ij}'S_{ij}'}\,, \tag{16}$$

where the second term on the right-hand side can be estimated from the total viscous dissipation rate of turbulent kinetic energy

$$\rho\epsilon = 2\mu\overline{S_{ij}'S_{ij}'} + 2\overline{\mu' S_{ij}'S_{ij}'}\,. \tag{17}$$

Gavrilov and Rudyak [24] assumed that since μ' can be either positive or negative whereas $S_{ij}'S_{ij}'$ is always positive, the second term in Eq. (17) will be small on average and therefore it can be neglected. DNS data of Singh et al. [28] confirm that such assumption is fairly acceptable when $n < 1$. On the other hand, for Bingham fluids ($n = 1$) this assumption seems incorrect. Nevertheless, for lack of knowledge of how to model such term we retain the assumption to be valid also for Bingham fluids. The main message is that larger modelling errors in the average viscosity should be expected for Bingham fluids.

In light on the above consideration, the second term of Eq. (16) can be approximated using Eq. (17),

$$2\overline{S_{ij}'S_{ij}'} \simeq \frac{\rho\epsilon}{\mu} = \frac{\rho\beta^*\omega k}{\mu}\,, \tag{18}$$

and substituting in Eq. (16) gives

$$\dot{\gamma}^2 = 2S_{ij}S_{ij} + \frac{\rho\beta^*\omega k}{\mu}\,. \tag{19}$$

Note that, in Eq. (15), μ is a function of $\dot{\gamma}$, which in turn is now a function of μ because of Eq. (19). In mathematical terms, $\mu = f(\mu)$, where $f(\mu)$ is the function obtained combining Eqs. (15) and (19). Since the governing equations are solved using iterative solution methods, the mean viscosity can be simply computed at each new outer iteration using μ from the previous iteration. However, to avoid possible numerical instabilities in the iterative solver due to the highly non-linear nature of $\mu = f(\mu)$, it is advised to perform a few intermediate iterations (e.g., using a simple fixed-point algorithm) before proceeding to the next outer iteration.

3.2. Closure for the non-Newtonian stress tensor

DNS for shear-thinning fluids [14,29] showed that μ'/μ does not exceed 30%. Thus, assuming small viscosity fluctuations, it is reasonable to relate μ' to the fluctuations of the deformation rate tensor as

$$\mu' \approx \frac{\partial\mu}{\partial S_{ij}}S_{ij}' = \frac{\partial\mu}{\partial\dot{\gamma}}\frac{\partial\dot{\gamma}}{\partial S_{ij}}S_{ij}' = \frac{\partial\mu}{\partial\dot{\gamma}}\frac{2S_{ij}}{\dot{\gamma}}S_{ij}'\,, \tag{20}$$

whence,

$$\tau_{ij}^{nn} = 2\overline{\mu' S'_{ij}} = 2\frac{\partial\mu}{\partial\dot{\gamma}}\frac{S_{ij}}{\dot{\gamma}}2\overline{S'_{ij}S'_{ij}}\,, \tag{21}$$

and by virtue of Eq. (18),

$$\tau_{ij}^{nn} = 2\frac{\partial\mu}{\partial\dot{\gamma}}\frac{S_{ij}}{\dot{\gamma}}\frac{\rho\beta^*\omega k}{\mu}\,. \tag{22}$$

The expression above can be rearranged in a more convenient form:

$$\tau_{ij}^{nn} = 2\mu^{nn}S_{ij}\,, \quad \mu^{nn} = \frac{\partial\mu}{\partial\dot{\gamma}}\frac{\rho\beta^*\omega k}{\mu\dot{\gamma}}\,, \tag{23}$$

where μ^{nn} can thus be interpreted as a turbulent non-Newtonian viscosity. For shear-thinning fluids μ^{nn} is always negative, thus it acts to reduce the turbulent transport of momentum.

3.3. Closure for the turbulence transport equations

The remaining terms that need to be modelled are χ^{nn}, $\mathscr{D}^{nn}$, ξ^{nn} and E^{nn}.

The first term is easily modelled by virtue of Eq. (20) as

$$\chi^{nn} = -2\overline{\mu' S'_{ij}}S_{ij} = -\mu^{nn}S^2\,. \tag{24}$$

For shear-thinning fluids this term is always positive and therefore it acts as a production term (see also Appendix B), even though it originates from the viscous term.

The second term, $\mathscr{D}^{nn}$, can be neglected since it is identical to the mean viscous transport term $\mathscr{D}$ but with the fluctuating viscosity instead of the mean viscosity. The smallness of this term is also confirmed by DNS [14,28].

Following the approach in [24], ξ^{nn} is modelled assuming that in the boundary layer the following approximations hold: $|\boldsymbol{u}| \approx u_1$, $S_{ij} \approx S_{12}$ and $k \approx \overline{u_1'^2}/2$, where 1 and 2 indicate the stream and cross-stream directions, respectively. Hence,

$$\begin{aligned}\xi^{nn} &= \frac{\partial(2\overline{\mu' u'_i}S_{ij})}{\partial x_j} \approx \frac{\partial}{\partial x_j}\left(2\frac{\partial\mu}{\partial\dot{\gamma}}\frac{2S_{kl}}{\dot{\gamma}}\overline{S'_{kl}u'_i}S_{ij}\right)\\ &\approx \frac{\partial}{\partial x_2}\left(2\frac{\partial\mu}{\partial\dot{\gamma}}\frac{2S_{12}^2}{\dot{\gamma}}\overline{S'_{12}u'_1}\right) = \frac{\partial}{\partial x_2}\left[\frac{\partial\mu}{\partial\dot{\gamma}}\frac{2S_{12}^2}{\dot{\gamma}}\left(\overline{u'_1\frac{\partial u'_1}{\partial x_2}} + \overline{u'_1\frac{\partial u'_2}{\partial x_1}}\right)\right]\\ &\approx \frac{\partial}{\partial x_2}\left(\frac{\partial\mu}{\partial\dot{\gamma}}\frac{2S_{12}^2}{\dot{\gamma}}\overline{\frac{\partial u'_1 u'_1/2}{\partial x_2}}\right) \approx \frac{\partial}{\partial x_2}\left(\frac{\partial\mu}{\partial\dot{\gamma}}\frac{2S_{12}^2}{\dot{\gamma}}\frac{\partial k}{\partial x_2}\right),\end{aligned} \tag{25}$$

and in its general form:

$$\xi^{nn} = \nabla\cdot\left(\frac{\partial\mu}{\partial\dot{\gamma}}\frac{S^2}{\dot{\gamma}}\nabla k\right). \tag{26}$$

For shear-thinning fluids, the quantity that multiplies ∇k is negative, thus acting as a reduction of the turbulent diffusion of k.

Finally, the last term that needs to be modelled is the non-Newtonian contribution to the transport equation of ω, E^{nn}. Since the ω-equation is empirical, this term is simply treated in analogy with the production term of the ω equation for the SST model, i.e.

$$E^{nn} = \frac{\rho\alpha}{\mu_t}(\xi^{nn} + \chi^{nn})\,, \tag{27}$$

where α is a closure coefficient of the k-ω SST model (see Appendix A).

3.4. Final mathematical model

The complete mathematical model reads:

$$\nabla\cdot\boldsymbol{u} = 0\,, \tag{28}$$

$$\frac{\partial(\rho\boldsymbol{u})}{\partial t} + \nabla\cdot(\rho\boldsymbol{u}\,\boldsymbol{u}) = \nabla\cdot\left[2(\mu + \mu_t + C_\tau\mu^{nn})\boldsymbol{S}\right] - \nabla(p + \frac{2}{3}k)\,, \tag{29}$$

$$\frac{D(\rho k)}{Dt} = \tilde{P}_k + D - \rho\epsilon + \xi^{nn} + \chi^{nn}\,, \tag{30}$$

$$\begin{aligned}\frac{D(\rho\omega)}{Dt} &= \rho\alpha S^2 + \nabla\cdot\left[(\mu + \sigma_\omega\mu_t)\nabla\omega\right] - \beta\rho\omega^2\\ &\quad + 2\rho(1 - F_1)\frac{\sigma_{\omega 2}}{\omega}\nabla k\cdot\nabla\omega + E^{nn}\,.\end{aligned} \tag{31}$$

$$D \equiv \nabla\cdot\left[(\mu + \sigma_k\mu_t)\nabla k\right], \tag{32}$$

$$\epsilon = \beta^*\omega k\,, \tag{33}$$

$$\dot{\gamma}^2 = 2S_{ij}S_{ij} + \frac{\rho C_\beta\epsilon}{\mu}\,, \tag{34}$$

$$\mu^{nn} = \frac{\partial\mu}{\partial\dot{\gamma}}\frac{\rho C_\beta\epsilon}{\mu\dot{\gamma}}\,, \tag{35}$$

$$\chi^{nn} = -C_\chi\mu^{nn}S^2\,, \tag{36}$$

$$\xi^{nn} = C_\xi\nabla\cdot\left(\frac{\partial\mu}{\partial\dot{\gamma}}\frac{S^2}{\dot{\gamma}}\nabla k\right), \tag{37}$$

$$E^{nn} = C_E\frac{\rho\alpha}{\mu_t}(\xi^{nn} + \chi^{nn})\,. \tag{38}$$

The original SST model and its closure coefficients are reported in Appendix A, whereas the closure coefficients relative to the new model (C_β, C_τ, C_χ, C_ξ and C_E) are given in Section 7.1.

The quantity $\partial\mu/\partial\dot{\gamma}$ depends on the rheological model at hand. For the Herschel–Bulkley model with the Papanastasiou regularisation it reads:

$$\frac{\partial\mu}{\partial\dot{\gamma}} = \frac{(n-1)K\dot{\gamma}^n - \tau_0(1 - e^{-m\dot{\gamma}}) + m\dot{\gamma}\tau_0 e^{-m\dot{\gamma}}}{\dot{\gamma}^2}\,. \tag{39}$$

Finally, for the boundary conditions on perfectly smooth walls, the same conditions of the standard SST model can be applied because all the non-Newtonian contributions (μ^{nn}, χ^{nn}, ξ^{nn} and E^{nn}) are zero at the wall (for χ^{nn} and ξ^{nn}, see Appendix B).

4. Pipe flow simulations: test cases, computational domain and boundary conditions

The new model, hereafter labelled as 'SST-HB', has been calibrated on DNS data [14,28,29] for fully-developed flows in smooth pipes of power-law (PL), Bingham (Bn) and Herschel–Bulkley (HB) fluids. Furthermore, as anticipated in the introduction, the performance of three Newtonian eddy-viscosity models is investigated. The selected models are the $k-\omega$ SST [25], the k-$\sqrt{k}L$ [30] and the Spalart–Allmaras [31] models. These will be hereafter referred to as SST, KSKL and SA, respectively.

4.1. Test cases

The definition of the Reynolds number for Herschel–Bulkley fluids is difficult because the choice of the viscosity is not univocal. For pipe flows, a standard choice is to use the wall kinematic viscosity, that for Herschel–Bulkley fluids reads

$$\nu_w = \frac{\tau_w}{\rho}\left(\frac{K}{\tau_w - \tau_0}\right)^{1/n}, \tag{40}$$

where τ_w is the shear stress at the wall. For a pipe having diameter $D = 2R$, with the Cartesian axes at centre of the pipe and with the z-axis aligned with the flow, τ_w is related to the pressure gradient $\partial p/\partial z$ inside the pipe as

$$\tau_w = \frac{R}{2}\frac{\partial p}{\partial z}\,. \tag{41}$$

From the wall viscosity, the Reynolds number can be thus defined as

$$Re_w = \frac{U_b D}{\nu_w}\,, \tag{42}$$

Table 1
Summary of the considered test cases. Calculations were performed for each possible combination of rheology, Reynolds number and RANS model listed in the table.

Case	n	τ_0/τ_w (%)	Re_τ	Re_w (Nwt)	RANS model
Nwt	1.0	0	323	∼ 10 000	New model (SST-HB)
PL08	0.8	0	500	∼ 17 000	$k-\omega$ SST-2003 (SST)
PL06	0.6	0	750	∼ 27 000	Spalart–Allmaras (SA)
PL04	0.4	0	1000	∼ 37 000	$k-\sqrt{k}L$ (KSKL)
Bn5	1.0	5	1250	∼ 48 000	
Bn10	1.0	10	1500	∼ 59 000	
Bn20	1.0	20	2000	∼ 82 000	
Bn30	1.0	30	2500	∼ 105 000	
HB10	0.8	10			

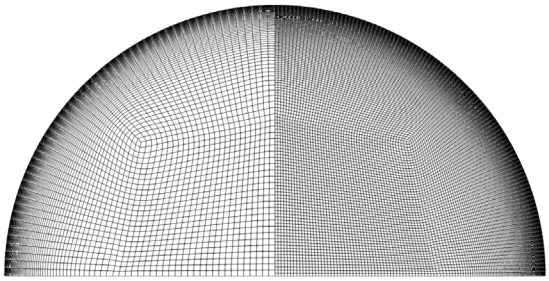

Fig. 1. One quarter of the coarsest and finest grid.

where U_b is the bulk velocity. The problem with this definition is that Re_w cannot be determined *a priori* because either U_b or ν_w is unknown before the simulation, depending on whether the pressure gradient or the flow rate is imposed. It is thus useful to introduce the friction Reynolds number,

$$Re_\tau = u_\tau R/\nu_w\,, \tag{43}$$

with $u_\tau = \sqrt{\tau_w/\rho}$ being the friction velocity. The latter is also used to define $u^+ = u/u_\tau$, $k^+ = k/u_\tau^2$ and the wall unit $y^+ = (R-r)u_\tau/\nu_w$, with $r = \sqrt{x^2+y^2}$.

The wall viscosity was chosen as $\nu_w = 1/Re_\tau$ and the non dimensional pressure gradient $(\partial p/\partial z)R/\tau_w$ was set equal to 2. From these non-dimensional parameters the fluid properties for each test case (Table 1) can be uniquely determined.

4.2. Computational domain and boundary conditions

The full pipe was discretised using four structured grids (Fig. 1) covering a refinement ratio of 2, with the finest grid made of about 86 000 cells (232 and 212 cells in the radial and azimuthal direction, respectively). The grid resolution at the pipe wall was chosen such that $y^+ \lesssim 0.1$ for all the considered test cases to ensure low levels of numerical uncertainty [35] (see Section 6).

Since the flow is fully developed, only one layer of cells was considered in the flow direction, and periodic boundary conditions were applied stream-wise. At the pipe wall ($x^2 + y^2 = R^2$), the impermeable/no-slip boundary conditions for the velocity ($\boldsymbol{u} = 0$) and the Neumann condition for pressure ($\partial p/\partial n = 0$) were applied. All the turbulence quantities except ω are set to zero at the wall. For ω, the following value is imposed at the first cell-centre away from the wall,

$$\omega = \frac{6\mu}{\rho\beta_1 d^2}\,, \tag{44}$$

where d is the distance from the wall and $\beta_1 = 3/40$. The value of ω at the wall surface is set to ten times the value given by Eq. (44), as in the original SST model [36].

Table 2
Numerical uncertainty in the friction factor f for the finest grid in percentage of the simulated data.

	SST-HB	SST	SA	KSKL
$Re_\tau = 323$ ($y^+_{\max} = 0.016$)				
Nwt	0.21	0.21	0.04	0.08
PL04	0.17	0.19	0.02	0.03
Bn20	0.19	0.21	0.03	0.07
HB10	0.28	0.21	0.05	0.11
$Re_\tau = 2500$ ($y^+_{\max} = 0.125$)				
Nwt	1.37	1.37	0.03	0.30
PL04	1.21	1.33	0.07	0.01
Bn20	1.26	1.33	0.02	0.03
HB10	1.28	1.35	0.02	0.07

5. Flow solver

The CFD code used for the present work is ReFRESCO [37], a viscous-flow code currently being developed and verified for maritime purposes by the Maritime Research Institute of the Netherlands (MARIN) in collaboration with several non-profit organisations around the world. The code solves incompressible Reynolds-averaged momentum and continuity equations in combination with transport equations for turbulence quantities. A number of other features such as multiphase and cavitation models are also included but they are not considered in the present work. Originally developed for Newtonian fluids, ReFRESCO has been recently extended and verified [38] for flow simulations of Herschel–Bulkley fluids.

Equations are discretised in strong-conservation form with a second-order finite-volume method for unstructured mesh with cell-centred co-located variables. Mass conservation is ensured with a pressure-correction equation based on a SIMPLE-like algorithm [39]. The convective fluxes of all transport equations are linearised with the Picard method and discretised with the Harmonic scheme [40].

6. Numerical uncertainties

For a meaningful comparison with data from the literature, it is important to ensure that the numerical errors/uncertainties are sufficiently small.

For statistically steady flows, it is commonly accepted to divide numerical errors in three categories: discretisation, iterative and round-off errors. Round-off errors are due to the finite precision of computers and they can be safely neglected for the present work by using double precision. Iterative errors are due to the use of iterative methods to find the solution of the discretised equations. These can be neglected by reducing residuals to machine accuracy, although less strict criteria are usually sufficient for practical applications. For the present work, calculations were stopped when the L_2 norm of the normalised residuals was below 2×10^{-10}, which was observed to be sufficient to safely neglect the contribution of iterative errors. We have thus assumed that the numerical uncertainties are only due to discretisation errors.

The discretisation uncertainties in the friction factor $f = 2\tau_w/(\rho U_b^2)$ were estimated using the method of Eça and Hoekstra [41] and they are reported in Table 2 for the lowest and highest Reynolds numbers considered in this work. Among the three Newtonian eddy-viscosity models, the SST model has clearly the largest uncertainties, confirming the observations made in [35]. Overall, the discretisation uncertainties never exceed 1.4%, and they are only slightly affected by the fluid rheology.

It is anticipated that, for Bingham and Herschel–Bulkley fluids, the Newtonian RANS models incorrectly predict a plug region (see Sections 7.2 and 7.4), i.e. a region with $\dot\gamma = 0$. This means that the regularisation is activated and the choice of the regularisation parameter, m, influences the numerical solution. In general, the regularisation parameter must be chosen large enough to avoid large regularisation

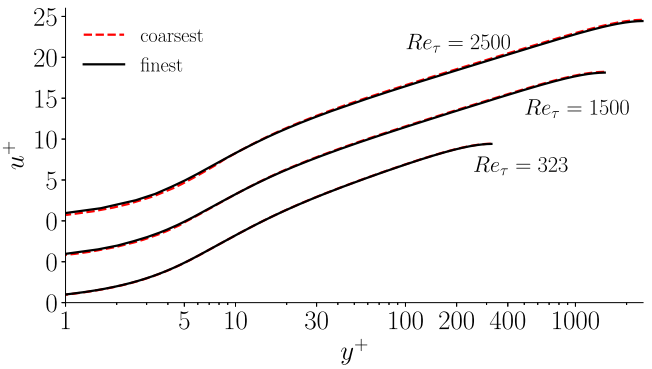

Fig. 2. Mean velocity profiles on the coarsest and finest grids for Newtonian fluids using the SST model.

errors, but not too large to compromise the convergence of the iterative solver. For the present calculations, the regularisation parameter was chosen such that $M \equiv \tau_0 m/(\rho \nu_w) \approx 2000$. The sensitivity of the friction factor due to the regularisation parameter was assessed by varying M from 2000 to 500, and the maximum difference in the friction factor among all the test cases never exceeded 0.1%. With the new model, on the other hand, the average shear rate was actually never low enough to activate the regularisation (thanks to the second term in Eq. (34)). Therefore, both the solution and the iterative convergence were totally unaffected by the choice of m.[2] In summary, it is reasonable to consider the numerical uncertainty to be within 1.4% of the friction factor.

For the mean velocity profiles, only small differences between the solution on the coarsest and finest grids were observed, and mainly in the viscous sublayer at high Reynolds numbers (see Fig. 2). Thus, in conclusion, the numerical uncertainties are sufficiently small to allow a meaningful comparison with data from the literature.

7. Results and discussion

7.1. Model calibration

In order to achieve a wide range of applicability for the new model, the closure coefficients were chosen to provide satisfactory agreement with DNS data [14,28,29], for a total of 10 test cases. Furthermore, little adjustments in the closure coefficients were made to improve the agreement with correlations from the literature for the friction factor [42,43] at higher Reynolds numbers. The final selected closure coefficients are:

- $C_\beta = 0.667$, $C_\tau = 0.6$, $C_\chi = 0.6$, $C_\xi = 0.4$
- $C_E = C_{E1} F_E(n) + C_{E2}(1 - F_E(n))$
- $C_{E1} = 2.5$, $C_{E2} = 1.85$
- $F_E(n) = 0.5 \tanh\left[8(n - 0.75)\right] + 0.5$

Among the large number of combinations of closure coefficients that provided satisfactory agreement with data from the literature, the set with the lower coefficients was favoured. In this way, the modification of the SST model is minimised, and so is the impact of the additional terms on the iterative solver.

It was also decided to use a blending function, F_E, such that C_E yields values from C_{E1} to C_{E2} when the flow index n goes from 1 to 0.4. The reason for this is that C_{E1} was observed to be optimal as long as $0.8 \le n \le 1$, whereas for $n < 0.8$ the effect of E^{nn} on the numerical solution became excessive, especially at high Reynolds numbers. F_E was thus devised to reduce E^{nn} for $n < 1$. In practice, since $E^{nn} > 0$ for the tested rheologies, F_E reduces the extra production of ω for low values of the flow index.

It is finally remarked that the blending functions F_1 and F_2 stemming from the original SST model (see also Appendix A) have not been modified for the new model. However, these functions contain the molecular viscosity and, since they were originally designed for Newtonian fluids, they may not always work as intended when using non-Newtonian fluids. For pipe flows, these functions are virtually constant (equal to one) across the pipe section, thus no issues were encountered. On the other hand, further research is needed to verify this on more complex wall-bounded flows, for example with adverse pressure gradient and flow separation.

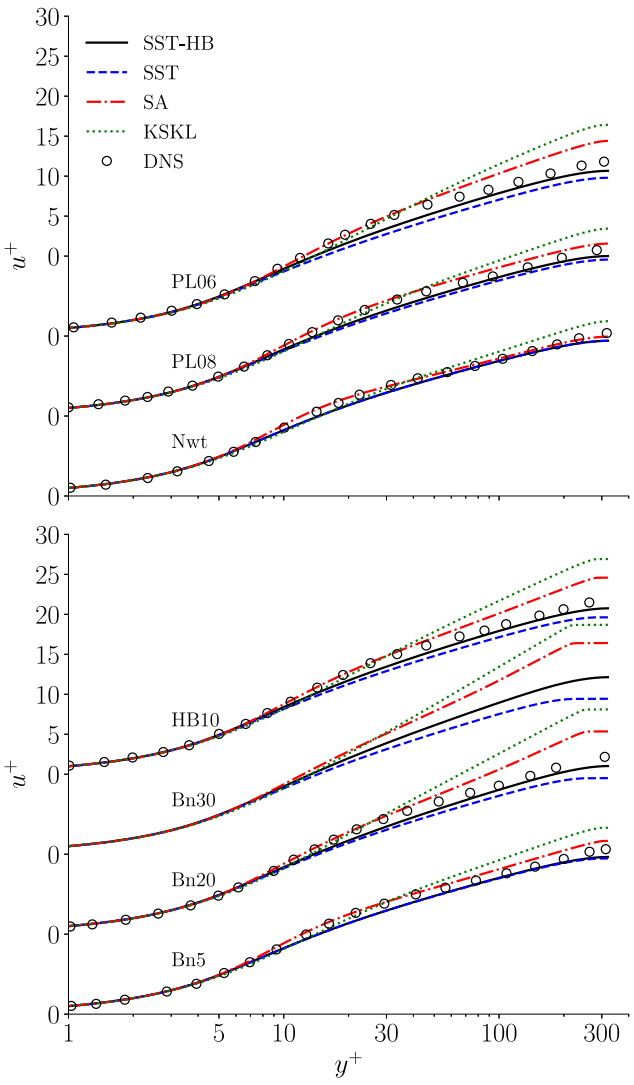

Fig. 3. Mean velocity profiles for $Re_\tau = 323$.
Source: DNS data are from [28] and do not include the case Bn30.

7.2. Mean velocity

The mean velocity profiles for $Re_\tau = 323$ are shown in Fig. 3. For Newtonian fluids (Fig. 3 top), the SST and SST-HB produce identical results, as expected, and the SA shows the best agreement with DNS, even in the buffer layer ($5 < y^+ < 30$).

[2] This is true as long as m is sufficiently large; too low values may still influence the solution. Also, for external flows, the region outside the boundary layer is typically undeformed, so the iterative solver may still be affected by the use of large regularisation parameters.

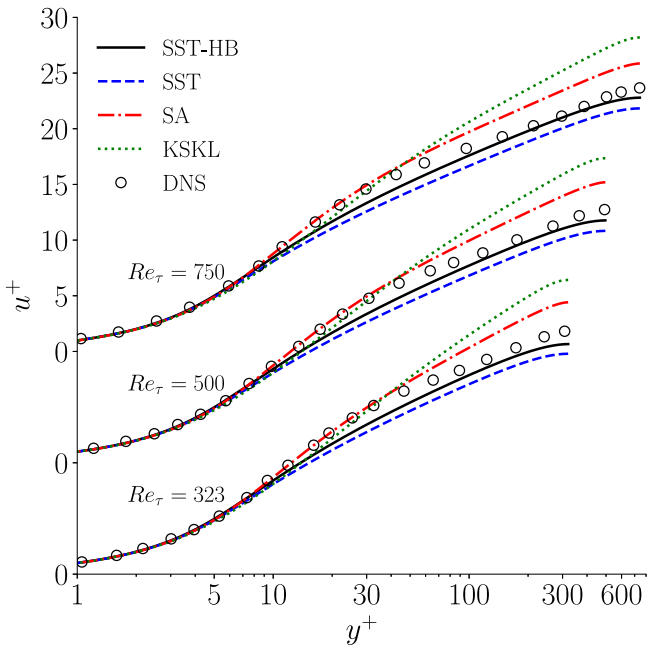

Fig. 4. Mean velocity profiles for PL06 at $Re_\tau = 323, 500, 750$.
Source: DNS data are from [29].

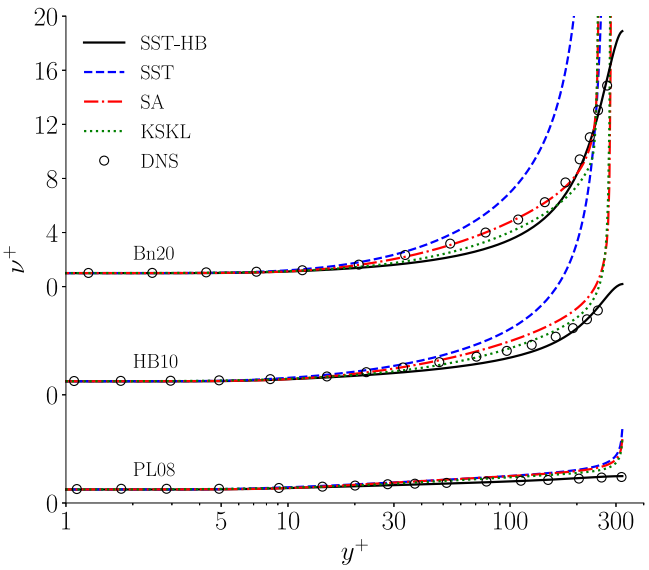

Fig. 5. Average viscosity for $Re_\tau = 323$.
Source: DNS data are from [28].

For the non-Newtonian cases, the new model produces the best agreement with DNS, although some discrepancies are noticeable around $y^+ = 30$. However, such discrepancies occur also for Newtonian fluids, so they are not strictly related to the non-Newtonian closure.

The Newtonian RANS models KSKL and SA tend to overpredict the mean velocity, meaning higher flow rates and lower friction factors, whereas the SST model seems rather insensitive to the non-Newtonian character of the fluid, which results in an underprediction of the mean velocity profile. Interestingly, for Bingham and Herschel–Bulkley fluids, the Newtonian RANS models incorrectly predict flat velocity profiles near the centreline (especially visible for Bn20 and Bn30), which indicates the presence of an unyielded region, or 'plug'. This plug is caused by the very large viscosity in the core region (see also Section 7.3) and it characterised by zero mean shear rate.[3] Unyielded plugs are typical of laminar flows of yield-stress fluids in pipes and channels. For turbulent flows, both DNS [13,28] and experimental data [44,45] suggest that the solid plug at the core is broken once the flow becomes turbulent. For viscoplastic fluids with truly time-independent rheology, plugs smaller than the Kolmogorov scales may still exist where the instantaneous shear rate is zero.

Unfortunately, DNS data for $Re_\tau > 323$ are only available for power-law fluids. Nevertheless, the agreement of the SST-HB model with the DNS appears to slightly improve for $Re_\tau = 750$ (Fig. 4), whereas no discernible improvements are observed for the SST, SA and KSKL models.

7.3. Average viscosity

The average viscosity predicted by the SST-HB model compares well with DNS, although the agreement seems to deteriorate for yield stress fluids (see Fig. 5). In the core region, the SST-HB clearly outperforms the other models. In particular, the Newtonian turbulence models predict a very large viscosity near the centreline of the pipe, as a result of the (nearly) zero mean shear rate. Remarkably, for Bn20 and $y^+ < 200$, the SA model agrees very well with DNS. However, this seems rather a fortuity since such good agreement is not observed in the other test cases.

While the new model produces the best agreement among the considered eddy-viscosity models, a clear discrepancy is noticeable for $20 < y^+ < 200$ for Bn20 and HB10. This could be explained by looking at the two main assumptions underlying the average viscosity model.

The first assumption is Eq. (15). From the mathematical standpoint, this assumption is exact when the viscosity is either a constant or a linear function of the instantaneous shear rate $\dot{\gamma}$. For power-law fluids, the viscosity is proportional to $\dot{\gamma}^{n-1}$, therefore the lower the flow index n the more the assumption becomes weak. In the limit of $n = 0$, the viscosity is proportional to $\dot{\gamma}^{-1}$, as for Bingham fluids. This means that for Bingham fluids this assumption is always weaker than for power-law fluids. The second assumption concerns the mean shear rate $\dot{\gamma}^2 = 2S_{ij}S_{ij} + 2\overline{S'_{ij}S'_{ij}}$. The last term was approximated using the mean dissipation rate of TKE, assuming that $\overline{\mu' S'_{ij} S'_{ij}} \approx 0$. DNS [28] showed that the latter term is not negligible for Bingham fluids, especially for $20 < y^+ < 200$. In light of these considerations, it is plausible that the average viscosity model performs less well for Bingham fluids and for $20 < y^+ < 200$.

It is finally remarked that viscosity is especially important near the wall, where the viscous stresses are dominant. Thus, outside the wall region ($y^+ > 10$), the small viscosity errors just mentioned above do not influence the mean velocity profile [46].

Fig. 6 shows that, for power-law fluids, the agreement of the SST-HB model with DNS is qualitatively the same for all Reynolds numbers, suggesting that the average viscosity model of Gavrilov and Rudyak [24] may be suitable also for calculations at higher Reynolds numbers.

To summarise, the new SST-HB model well predict the average viscosity for power-law fluids, also at different Reynolds numbers. For Bingham and Herschel–Bulkley fluids, the viscosity predicted by the SST-HB model shows some discrepancies with DNS, but these discrepancies are small and outside the wall region, thus they do not affect the mean flow. The main benefit of the new model is the significant reduction of large viscosity errors in the core region. This prevents the formation of unphysical plugs for yield-stress fluids, with positive effects also on iterative convergence (see Appendix C).

[3] For the present calculations, the mean shear rate is actually close to zero but not exactly zero because of the use of the regularisation.

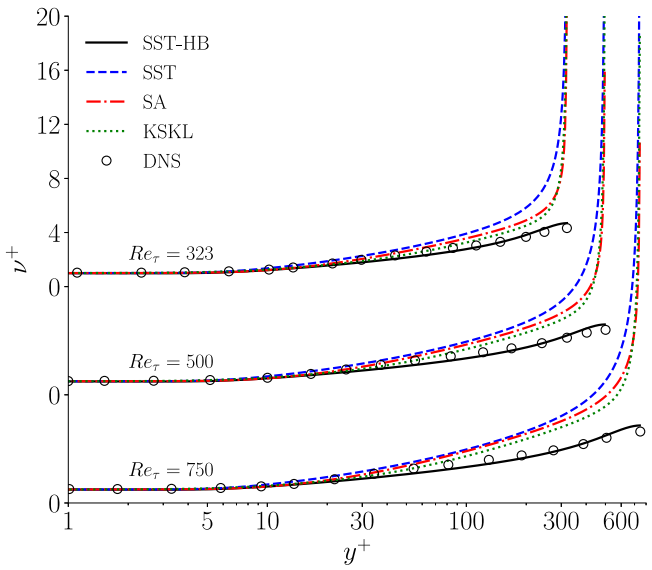

Fig. 6. Average viscosity for PL06 at different Reynolds numbers.
Source: DNS data are from [29].

7.4. Mean shear stress budget

The total mean shear stress written in cylindrical coordinates reads:

$$\tau_{zr}^{tot} = \mu \frac{du_z}{dr} - \overline{u_r' u_z'} + \overline{\mu' S_{zr}'}, \tag{45}$$

where z and r indicate the axial and radial direction, respectively, and the terms on the right-hand side are the viscous, turbulent and non-Newtonian stresses. For the SST-HB model, the total mean shear stress is modelled as (subscripts are omitted)

$$\tau^{tot} = \mu \frac{du_z}{dr} + \mu_t \frac{du_z}{dr} + \mu^{nn} \frac{du_z}{dr} \equiv \tau^{v} + \tau^{t} + \tau^{nn}, \tag{46}$$

whereas for the Newtonian eddy-viscosity models the last component is zero. Integrating in the radial direction of the momentum equation in the axial direction and using the non-dimensional wall coordinates leads to

$$\tau^{tot+} = 1 - \frac{y^+}{Re_\tau}. \tag{47}$$

This means that the distribution of the mean viscous, turbulent and non-Newtonian shear stresses can be a function of the fluid rheology, but the total shear stress must always vary linearly across the pipe diameter. The total mean shear stress and its components are plotted in Fig. 7 for $Re_\tau = 323$.

For Newtonian fluids, all models produce a fairly good prediction of τ^v and τ^t, with some loss of accuracy in the buffer layer ($5 < y^+ < 30$). For non-Newtonian fluids, the SST, SA and KSKL models poorly predict all the shear stress components. In particular, for Bingham and Herschel–Bulkley fluids, the viscous stress predicted by these models has an unexpected local peak (at $y^+ \approx 250$ for Bn20, see Fig. 7 c), which alters the correct linear distribution of the total stress over the pipe diameter. The position of this incorrect peak is in proximity of the plug, where the velocity gradient and the viscosity have a steep variation in a relative short distance, causing large discretisation errors. These errors could be reduced by locally refining the grid around the plug, but note that results would still be physically incorrect.

The SST-HB has clearly the best agreement with DNS for all the shear stress components, and the total stress follows the expected linear behaviour for all test cases. Furthermore, the non-Newtonian shear stresses, τ_{ij}^{nn}, are very well captured by the SST-HB model, except in the viscous sublayer. This is because $\mu^{nn} \propto \omega k$ (see Eq. (35)) and the turbulent kinetic energy is set to zero at the wall. In any case, in the viscous sublayer the total stress is completely dominated by the viscous component, therefore the effects of this deficiency on the numerical solution are expected to be small.

7.5. Turbulent kinetic energy

All eddy-viscosity models are clearly unable to accurately predict the distribution of TKE (Fig. 8), even for Newtonian fluids.[4] According to DNS for shear-thinning and viscoplastic fluids, the peak of k should increase. However, the SST, SA and KSKL models predict a decrease of k. While the new SST-HB is also unable to capture the peak of k, it is capable, at least, of maintaining a higher level of turbulent kinetic energy compared to the other turbulence models. This is possible thanks to the χ^{nn} term in the k-equation, which acts as a production of turbulent kinetic energy (see Appendix B).

The poor prediction of k is an expected limitation of two-equation turbulence models. In fact, for increasing shear-thinning effects, k increases and μ_t decreases, whereas two-equation models imply direct proportionality between μ_t and k. Nevertheless, the accurate prediction of k is often not of importance for many engineering applications, which are usually interested in the mean velocity and pressure profiles and in the friction factor.

Finally, the incorrect plug region already discussed in the previous sections is visible also in Fig. 8(c) for the SA and KSKL models, showing zero turbulent kinetic energy for $y^+ \gtrsim 250$. Despite that the plug was predicted also by the SST model, the turbulent kinetic energy is however not zero for this model, which is physically inconsistent.

In summary, the SST-HB always predict a higher level of k among the considered turbulence models, and its accuracy is unsatisfactory yet comparable with that of the SST model when the latter is applied to Newtonian fluids.

7.6. Friction factor

The friction factor, f, is often one or even the only quantity of interest for many engineering applications. It is therefore an important quantity to assess the performance of the new model.

The comparison of the friction factor, f, with DNS is reported in Table 3. The difference Δf reflects the predictions of the mean velocity profiles already observed in Section 7.2: SA and KSKL under predict f (U_b is larger), vice-versa for SST.

The SST-HB model undoubtedly provides the best prediction for all the test cases, especially at the higher Reynolds numbers. While the difference of 14.3% for PL04 is considerable, it is still the smallest among all turbulence models. Such difference could be easily reduced by increasing, for example, the calibration coefficient C_{E2} (see Section 7.1) from 1.85 to 2.0. By doing so, however, the accuracy for power-law fluids at higher Re_τ would deteriorate. It was thus decided to sacrifice some accuracy at $Re_\tau = 323$ in favour of more consistent accuracy for a wide range of Reynolds numbers.

In order to assess the new model also for $Re_\tau > 750$, the friction factor has been compared against correlations from the literature. For power-law fluids, two correlations were considered. The first [42] reads

$$f = \left(0.102 - 0.033n + \frac{0.01}{n}\right) \frac{1}{Re_{MR}^{\frac{1}{2(n+1)}}}, \tag{48}$$

where Re_{MR} is the Reynolds number defined by Metzner and Reed [48],

$$Re_{MR} = \frac{8\rho U_b^{2-n} D^n}{K(6+2/n)^n}, \tag{49}$$

[4] This was already observed by Wilcox [47] for the $k-\omega$ model. Despite the poor prediction of k (and ϵ), Wilcox showed that the velocity profile and the skin friction were well predicted for both external and internal flows.

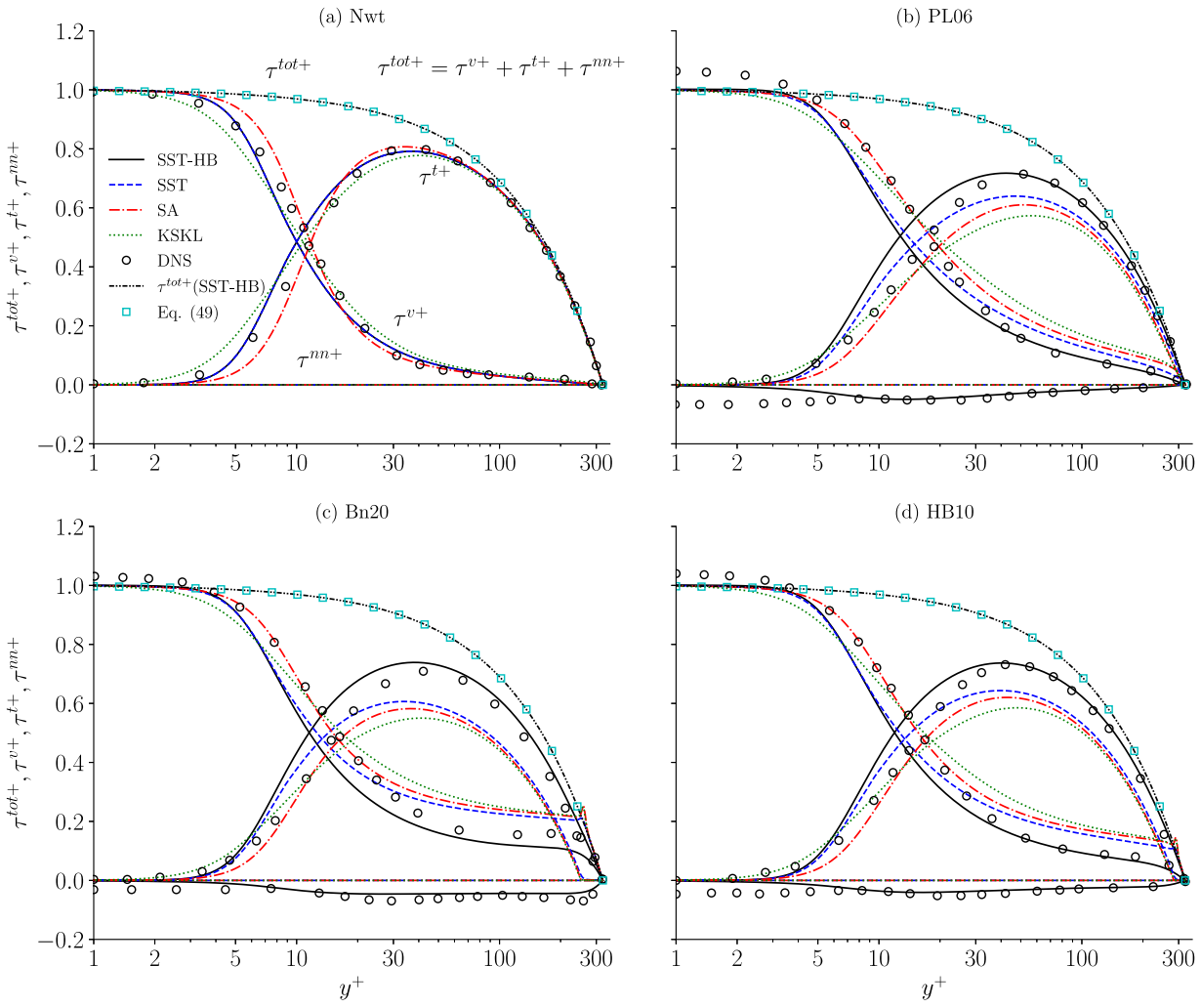

Fig. 7. Mean shear stress budget at $Re_\tau = 323$ obtained with the four eddy-viscosity models and from DNS [14,28]. The total mean shear stress τ_{tot} is relative to the SST-HB model.

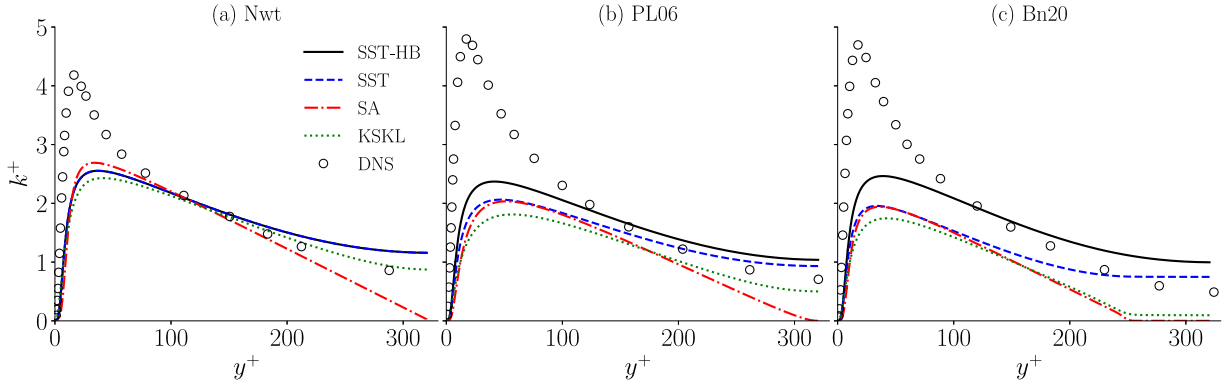

Fig. 8. Turbulent kinetic energy for $Re_\tau = 323$.
Source: DNS data are from [28].

also called Metzner–Reed Reynolds number. Note that, for a particular rheology, higher Re_{MR} means also higher Re_τ, thus the following discussion is valid for both Reynolds numbers. The second correlation [43] reads

$$f = 0.079\left[\frac{Re_{MR}}{8}(6+2/n)^n\right]^{\frac{-1}{2(n+1)}}. \tag{50}$$

Both correlations are plotted in Fig. 9, together with DNS (open symbols) and RANS data (filled symbols). The maximum difference between DNS and the correlations is about −3.5%, which can be seen as a coarse indication of the correlation's uncertainty.

The new model (Fig. 9 d) well predicts f for power-law fluids also at high Reynolds numbers. At $Re_\tau = 2500$, the maximum difference relative to the first and second correlations is −2.7% and −6.1%, respectively. Compared to SST, the benefits of using the new model are

Table 3
Friction factor $f = 2\tau_w/(\rho U_b^2)$ from DNS [14,28,29] and from eddy-viscosity models of the present work. The difference Δf is relative to DNS.

	Case	DNS	SST-HB		SST		SA		KSKL	
		$f \times 10^3$	$f \times 10^3$	Δf (%)	$f \times 10^3$	Δf (%)	$f \times 10^3$	Δf (%)	$f \times 10^3$	Δf (%)
$Re_\tau = 323$	Nwt	7.88	8.264	4.9	8.264	4.9	7.819	−0.8	7.203	−8.6
	PL08	7.36	7.831	6.5	8.219	11.7	6.786	−7.7	6.291	−14.5
	PL06	6.74	7.422	10.2	8.134	20.7	5.734	−14.9	5.227	−22.4
	PL04	5.95	6.797	14.3	7.982	34.2	4.971	−16.4	4.710	−20.8
	Bn5	7.70	8.120	5.5	8.176	6.2	7.055	−8.3	6.378	−17.1
	Bn10	7.36	7.879	7.1	8.092	10.0	6.390	−13.1	5.597	−23.9
	Bn20	6.74	7.270	7.9	7.942	17.9	5.499	−18.4	4.694	−30.3
	HB10	6.88	7.381	7.3	8.062	17.2	5.789	−15.9	5.089	−26.0
$Re_\tau = 500$	Nwt	6.89	7.108	3.2	7.108	3.2	6.889	0.0	6.279	−8.8
	PL06	5.86	6.332	8.0	6.981	19.1	4.965	−15.3	4.456	−24.0
$Re_\tau = 750$	Nwt	6.15	6.256	1.8	6.256	1.8	6.163	0.3	5.598	−8.9
	PL06	5.28	5.553	5.3	6.122	16.0	4.443	−15.8	3.941	−25.3

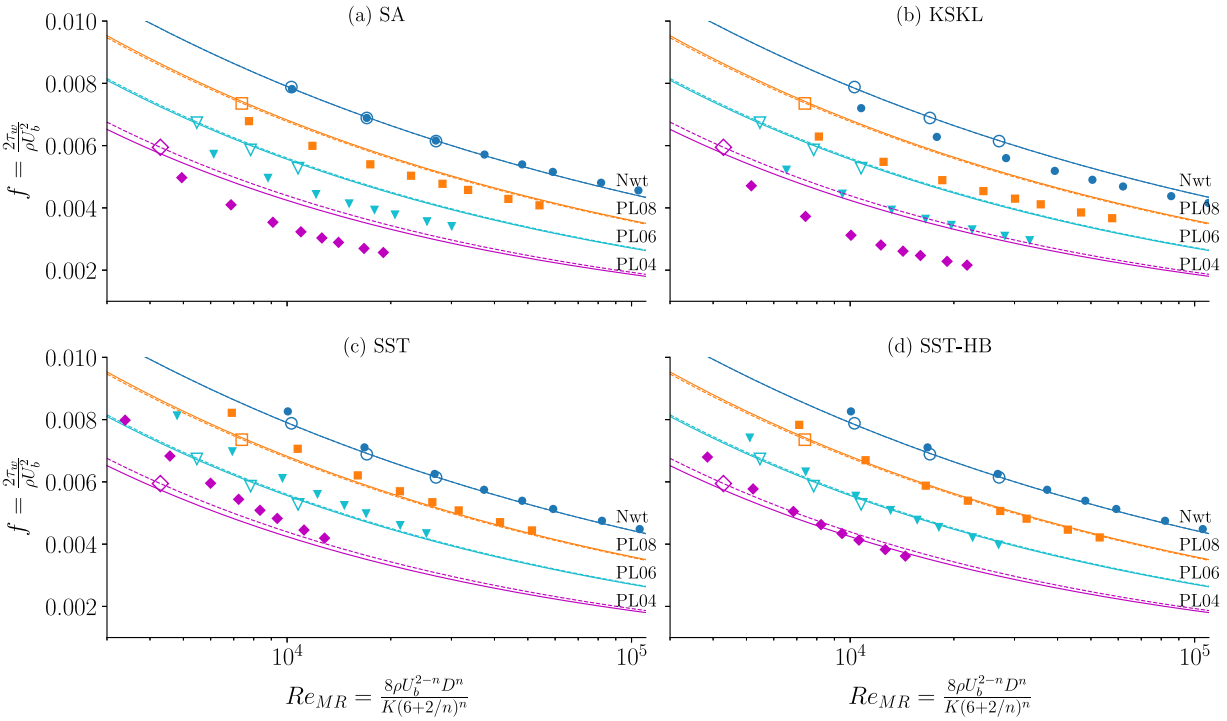

Fig. 9. Friction factor versus Re_{MR} for power-law fluids from present work (filled symbols), from DNS [14,29] (open symbols) and from the correlations of Anbarlooei et al. [42] (solid lines, Eq. (48)) and of Anbarlooei et al. [43] (dashed lines, Eq. (50)). The 8 points for each rheology correspond to $Re_\tau = 323, 500, 750, 1000, 1250, 1500, 2000, 2500$.

more evident for highly shear-thinning fluids. In fact, the accuracy of SST may be actually considered acceptable for moderate shear-thinning fluids, especially at high Reynolds numbers, where non-Newtonian effects become less important. To some extent, this is also true for the SA model (Fig. 9a), whereas it is clearly not true for the KSKL model (Fig. 9b), which significantly under predicts the friction coefficients for all Re_{MR}. Actually, KSKL appears to be rather inaccurate also for Newtonian fluids. This is surprising as KSKL proved to perform well for external wall bounded flows of Newtonian fluids (e.g. [49,50]). Fig. 9(b) suggests that KSKL may perform better at higher Reynolds numbers.

For Bingham fluids, two correlations [43,51] were considered, both having the following form

$$f = \frac{0.316}{4\sqrt{2}} \sqrt{\sqrt{\frac{He^2}{Re_G^4} + \frac{4}{Re_G}} + \frac{He}{Re_G^2}} - C\frac{He}{Re_G^2}, \tag{51}$$

where $Re_G = \rho U_b D/K$ is the generalised Reynolds number and $He = \rho\tau_0 D^2/K^2$, the latter being the Hedstrom number. The correlation reduces to the Blasius formula for $He = 0$, i.e. for zero yield stress.

In the earlier version [51] the coefficient C is equal to 2, whereas the later version [43] does not include the last term ($C = 0$). When these correlations were compared with the DNS data of Singh et al. [28], the maximum difference using $C = 2$ was around +10%, whereas with $C = 0$ the maximum difference was about –10%. We have thus deliberately opted for the middle way, i.e. $C = 1$, which has decreased the maximum difference down to 1.7% (see Table 4). This has increased the confidence in the correlation as being a more reliable representation of DNS data, nonetheless the comparison must be interpreted with the due caution.

Keeping the above considerations in mind, Table 4 shows the comparison of the present results against Eq. (51) with $C = 1$. The SST model appears to be suitable for weakly non-Newtonian fluids ($\tau_0/\tau_w = 10\%$) and for high Reynolds numbers, whereas the SA and KSKL models seem to perform poorly for Bingham fluids, at any flow regime.

The new model, on the other hand, seems to well predict f at all Reynolds numbers. However, the important finding here is that, for $Re_\tau > 323$, the new model appear to maintain approximately the same level of accuracy, without any marked change in $\Delta f(\%)$. This suggests that the model may be suitable for viscoplastic flows for a

Table 4
Difference $\Delta f(\%)$ of the friction factor relative to Eq. (51) with $C = 1$. DNS data are from [28].

		DNS	SST-HB	SST	SA	KSKL
$Re_\tau = 323$	Nwt	0.5	4.7	4.7	−0.2	−7.1
	Bn5	1.7	6.7	7.3	−5.9	−14.0
	Bn10	1.0	7.5	10.2	−11.1	−21.2
	Bn20	−0.1	7.4	16.8	−17.5	−28.8
	Bn30	–	6.16	24.94	−19.48	−28.68
$Re_\tau = 750$	Nwt	−0.2	1.3	1.3	0.0	−8.0
	Bn5	–	2.5	3.4	−6.3	−15.7
	Bn10	–	2.5	5.6	−13.9	−25.4
	Bn20	–	1.4	10.9	−24.1	−37.5
	Bn30	–	−0.78	17.45	−29.10	−41.11
$Re_\tau = 1500$	Nwt	–	1.3	1.3	1.8	−6.4
	Bn5	–	2.1	3.0	−4.3	−14.6
	Bn10	–	1.8	4.9	−13.4	−25.8
	Bn20	–	0.2	9.2	−26.2	−40.9
	Bn30	–	−2.73	14.64	−32.91	−46.37
$Re_\tau = 2500$	Nwt	–	2.3	2.3	3.9	−4.2
	Bn5	–	2.9	3.8	−1.9	−12.7
	Bn10	–	2.5	5.3	−11.9	−25.1
	Bn20	–	0.5	9.1	−26.5	−42.0
	Bn30	–	−2.96	13.78	−34.34	−48.68

wide range of Reynolds numbers. For a more compelling validation, however, DNS data for Bingham and Herschel–Bulkley fluids at high Reynolds numbers and with higher level of yield stress are needed. This is an important issue for future research.

8. Conclusions

A new turbulence model for Herschel–Bulkley fluids (and their special cases, i.e. Bingham and power-law) has been derived by modifying the popular $k-\omega$ SST model. The derivation was carried out along the lines of Gavrilov and Rudyak [24], who developed a turbulence closure for power-law fluids. The calibration coefficients were chosen to ensure satisfactory agreement with DNS data and with correlations for shear-thinning and yield-stress fluids for a wide range of Reynolds numbers. Furthermore, we have assessed three widely-used RANS models for Newtonian fluids, namely the SST, the Spalart–Allmaras (SA) and the $k-\sqrt{k}L$ (KSKL) models. The main conclusions of this work are summarised as follows:

- The new model showed good agreement in the mean velocity, average viscosity, mean shear stress budget and friction factors as compared to DNS data. Furthermore, the new model appears to be always more accurate than the standard SST model.
- The new model is inadequate for applications that require and accurate prediction of the TKE. Nonetheless, the accuracy of the prediction is comparable to that of the other selected RANS models when applied to Newtonian flows.
- The friction factor predicted by the new model agrees well with both DNS and correlations for power-law and Bingham fluids.
- Among the three Newtonian RANS models, the SST proved to be most suitable for weakly non-Newtonian fluids ($n \geq 0.8$ and $\tau_0/\tau_w \leq 10\%$) and for high Reynolds numbers ($Re_\tau > 750$). The SST model tends to underpredict the mean velocity and to overpredict the friction factor. Vice-versa for SA and KSKL, with the latter giving the worst agreement for all test cases.
- For yield-stress fluids, the three Newtonian RANS models incorrectly predict a plug. This is not only physically incorrect, as proved by previous studies, but it may also lead to large discretisation errors and difficult iterative convergence. With the new model, on the other hand, no plugs were predicted and the iterative convergence did not show any difficulty (see Appendix C). This last feature can be particularly appreciated for viscoplastic fluids in complex geometries, where the combination of large yield stresses and the slowly converging SIMPLE-like algorithms could easily lead to stagnating/diverging iterative convergence.

Finally, a number of important limitations need to be considered. First, while only one new empirical function ($F_E(n)$) was needed in the SST-HB model to produce good agreement with DNS for pipe flows, further empirical modifications of the original SST model may still be required for complex applications, such as those with adverse pressure gradient and flow separation both in external and internal flow configurations. In this regard, further research is recommended to verify the accuracy and robustness of the new model in more complex flows. Second, the current study was limited to $Re_\tau > 323$, and the accuracy of the new model is expected to decrease at lower Reynolds numbers. Third, DNS data are also affected by numerical errors/uncertainties which, unfortunately, could not be found. It was thus implicitly assumed that these errors were small compared to the modelling errors. In order to overcome this aspect, it is recommended for future DNS to provide uncertainty estimates. Fourth, it remains a question whether the new model is suitable for fluids with high yield stress, both because no validation data is available and because the flow may become transitional/laminar in the core of the pipe, especially at lower Reynolds numbers. Nevertheless, the new model may be more robust than the other Newtonian RANS models tested in this work, if anything, because of the better iterative convergence. Further DNS investigations at $Re_\tau > 323$ and with higher yield stress levels will be of great help to develop and improve turbulence models for Herschel–Bulkley fluids.

The new model is simple and appealing for engineering applications concerned with turbulent wall-bounded flows of Herschel–Bulkley fluids, and its formulation can be easily adapted to other GN fluid models by modifying the expression of $\partial\mu/\partial\dot{\gamma}$.

Declaration of competing interest

The authors declare that they have no known competing financial interests or personal relationships that could have appeared to influence the work reported in this paper.

Acknowledgements

This research is funded by the Division for Earth and Life Sciences (ALW) with financial aid from the Netherlands Organization for Scientific Research (NWO) with Grant No.ALWTW.2016.029. The research is also supported by the Port of Rotterdam (PoR), MARIN and the Dutch Ministry of Economic Affairs. Calculations were performed on the Marclus4 (MARIN) cluster. This study was carried out within the framework of the MUDNET academic network: https://www.tudelft.nl/mudnet/.

Appendix A. $k-\omega$ SST (2003)

The $k-\omega$ SST model of Menter et al. [25] that is used as a baseline for the derivation of the new turbulence model is reported below.

$$\frac{D(\rho k)}{Dt} = \tilde{P}_k + \nabla\cdot\left[(\mu+\sigma_k\mu_t)\nabla k\right] - \rho\overbrace{\beta^* k\omega}^{\epsilon} \tag{A.1}$$

$$\frac{D(\rho\omega)}{Dt} = \rho\alpha S^2 + \nabla\cdot\left[(\mu+\sigma_\omega\mu_t)\nabla\omega\right] - \beta\rho\omega^2 + 2\rho(1-F_1)\frac{\sigma_{\omega 2}}{\omega}\nabla k\cdot\nabla\omega \tag{A.2}$$

$$F_1 = \tanh\left\{\min\left[\max\left(\frac{\sqrt{k}}{\beta^*\omega d}, \frac{500\nu}{d^2\omega}\right), \frac{4\rho\sigma_{\omega 2}k}{CD_{k\omega}d^2}\right]^4\right\} \tag{A.3}$$

d is the distance to the wall boundary.

$$CD_{k\omega} = \max\left(2\rho\sigma_{\omega 2}\frac{1}{\omega}\nabla k\cdot\nabla\omega, 10^{-10}\right) \tag{A.4}$$

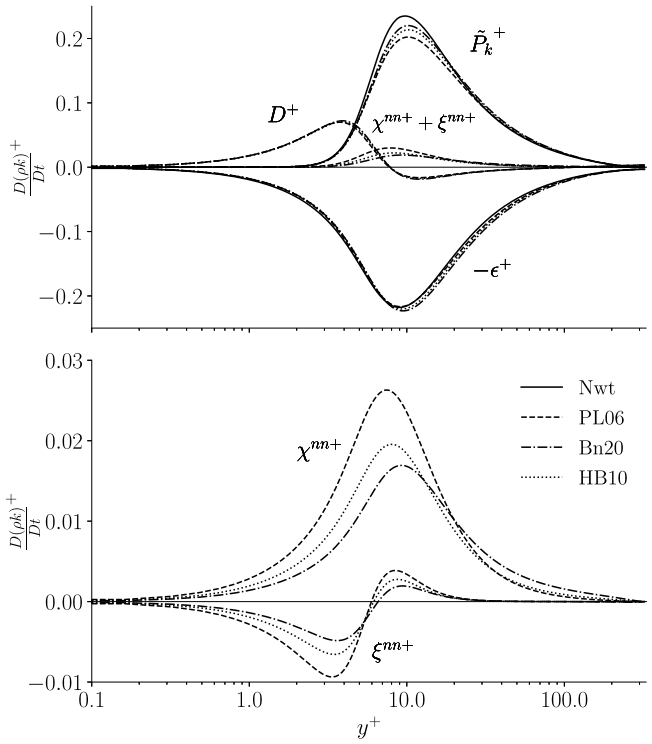

Fig. B.10. Production ($\tilde{P}_k^+$), dissipation (ϵ^+) and transport (D^+) of TKE (top) and non-Newtonian contributions (bottom) ($Re_\tau = 323$). The non-dimensional terms were obtained by dividing the dimensional terms by $\rho u_\tau^4/\nu_w$.

$$\nu_t = \frac{a_1 k}{\max(a_1\omega, SF_2)}, a_1 = 0.31 \tag{A.5}$$

$$F_2 = \tanh\left\{\left[\max\left(\frac{2\sqrt{k}}{\beta^*\omega d}, \frac{500\nu}{d^2\omega}\right)\right]^2\right\} \tag{A.6}$$

$$\tilde{P}_k = \min(\mu_t S^2, 10\beta^*\rho k\omega), \beta^* = 0.09 \tag{A.7}$$

$$\alpha = \alpha_1 F_1 + (1-F_1)\alpha_2, \quad \beta = \beta_1 F_1 + (1-F_1)\beta_2,$$
$$\sigma_k = \sigma_{k1} F_1 + (1-F_1)\sigma_{k2}, \quad \sigma_\omega = \sigma_{\omega1} F_1 + (1-F_1)\sigma_{\omega2},$$
$$\alpha_1 = 5/9, \quad \beta_1 = 3/40, \quad \sigma_{k1} = 0.85, \quad \sigma_{\omega1} = 0.5,$$
$$\alpha_2 = 0.44, \quad \beta_2 = 0.0828, \quad \sigma_{k2} = 1, \quad \sigma_{\omega2} = 0.856.$$

Appendix B. Non-Newtonian contributions in the TKE budget

In order to give an indication of the magnitude of the non-Newtonian contributions χ^{nn} and ξ^{nn} in the TKE equation, their distribution is plotted in Fig. B.10 together with the production, dissipation and transport terms (see also Eq. (30)). For non-Newtonian fluids, the difference between production and dissipation is absorbed by the non-Newtonian contributions, making the transport term D^+ nearly insensitive to the fluid rheology, in line with DNS data (Figs. 10 and 15 in [28]). The sum the non-Newtonian contributions is positive and appears to be larger for power-law fluids.

Appendix C. Iterative convergence

Fig. C.11 shows the iterative convergence of the residuals (top graph) with the new SST-HB and the standard SST model for Bn30 (most difficult case for iterative convergence), together with the estimated iterative error for the wall shear stress (bottom graph). The latter can be estimated since the pressure gradient is imposed and thus the exact wall shear stress is known. The wall shear stress requires

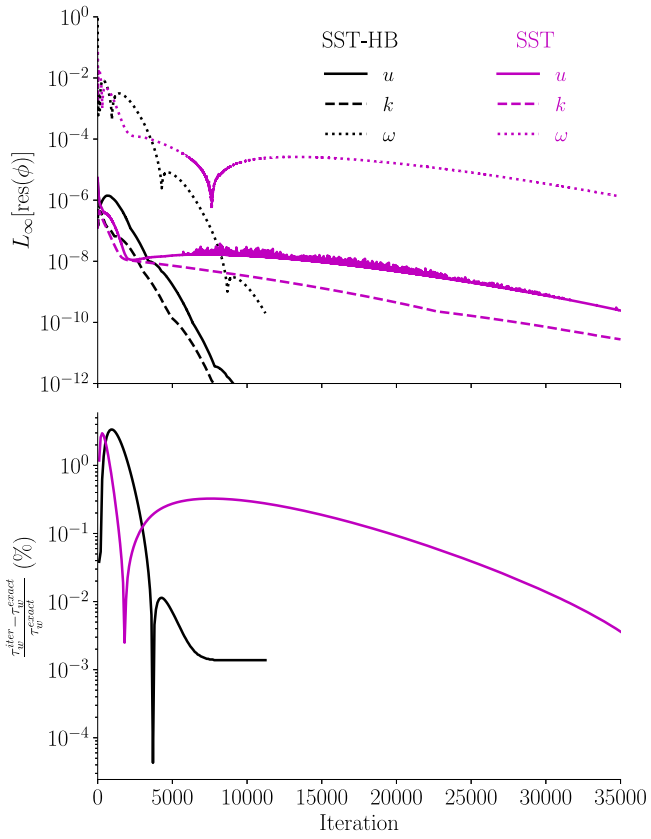

Fig. C.11. Iterative convergence of the L_∞ norm of the residuals (top) and wall shear stress error in percentage for the case $Re_\tau = 323$, Bn30 (bottom).

about 7000 iterations to convergence with the new model, whereas the standard SST (similarly for the SA and KSKL model) requires about 30 000 SIMPLE iterations. The better iterative convergence of the new model is simply due to the fact that the viscosity does not reach very large values in the core of the pipe, contrary to the other selected RANS models, which show an incorrect asymptote in the viscosity typical of laminar flows (see also Section 7.3), making the momentum equations stiffer and more difficult to solve.

References

[1] Z. Gao, H. Yang, M. Xie, Computation of flow around wigley hull in shallow water with muddy seabed, J. Coast. Res. 73 (June) (2015) 490–495, http://dx.doi.org/10.2112/SI73-086.1.
[2] S. Kaidi, E. Lefrançois, H. Smaoui, Numerical modelling of the muddy layer effect on Ship's resistance and squat, Ocean Eng. 199 (February) (2020) 106939, http://dx.doi.org/10.1016/j.oceaneng.2020.106939.
[3] N.S. Kelly, H.S. Gill, A.N. Cookson, K.H. Fraser, Influence of shear-thinning blood rheology on the laminar-turbulent transition over a backward facing step, Fluids 5 (2) (2020) 57, http://dx.doi.org/10.3390/fluids5020057.
[4] A. Busch, S.T. Johansen, Cuttings transport: On the effect of drill pipe rotation and lateral motion on the cuttings bed, J. Pet. Sci. Eng. (2020) http://dx.doi.org/10.1016/j.petrol.2020.107136.
[5] D. Mehta, A.K. Thota Radhakrishnan, J.B. van Lier, F.H. Clemens, Assessment of numerical methods for estimating the wall shear stress in turbulent Herschel–Bulkley slurries in circular pipes, J. Hydraul. Res. (2020) 1–18, http://dx.doi.org/10.1080/00221686.2020.1744751.
[6] F. Pinho, A GNF framework for turbulent flow models of drag reducing fluids and proposal for a k–ϵ type closure, J. Non-Newton. Fluid Mech. 114 (2–3) (2003) 149–184, http://dx.doi.org/10.1016/S0377-0257(03)00120-4.
[7] Y. Nagano, M. Hishida, Improved form of the k-ϵ model for wall turbulent shear flows, J. Fluids Eng. Trans. ASME (1987) http://dx.doi.org/10.1115/1.3242636.
[8] D. Cruz, F. Pinho, Turbulent pipe flow predictions with a low Reynolds number k–ϵ model for drag reducing fluids, J. Non-Newton. Fluid Mech. 114 (2–3) (2003) 109–148, http://dx.doi.org/10.1016/S0377-0257(03)00119-8.

[9] D. Cruz, F. Pinho, P. Resende, Modelling the new stress for improved drag reduction predictions of viscoelastic pipe flow, J. Non-Newton. Fluid Mech. 121 (2–3) (2004) 127–141, http://dx.doi.org/10.1016/j.jnnfm.2004.05.004.

[10] F.T. Pinho, C.F. Li, B.A. Younis, R. Sureshkumar, A low Reynolds number turbulence closure for viscoelastic fluids, J. Non-Newton. Fluid Mech. 154 (2–3) (2008) 89–108, http://dx.doi.org/10.1016/j.jnnfm.2008.02.008.

[11] P. Resende, K. Kim, B. Younis, R. Sureshkumar, F. Pinho, A FENE-p k–ϵ turbulence model for low and intermediate regimes of polymer-induced drag reduction, J. Non-Newton. Fluid Mech. 166 (12–13) (2011) 639–660, http://dx.doi.org/10.1016/j.jnnfm.2011.02.012.

[12] P.R. Resende, F.T. Pinho, B.A. Younis, K. Kim, R. Sureshkumar, Development of a low-Reynolds-number k-ω model for FENE-P fluids, Flow Turbul. Combust. 90 (1) (2013) 69–94, http://dx.doi.org/10.1007/s10494-012-9424-x.

[13] M. Rudman, H. Blackburn, Direct numerical simulation of turbulent non-Newtonian flow using a spectral element method, Appl. Math. Model. 30 (11) (2006) 1229–1248, http://dx.doi.org/10.1016/j.apm.2006.03.005.

[14] J. Singh, M. Rudman, H.M. Blackburn, The influence of shear-dependent rheology on turbulent pipe flow, J. Fluid Mech. 822 (2017) 848–879, http://dx.doi.org/10.1017/jfm.2017.296.

[15] G. Iaccarino, E.S. Shaqfeh, Y. Dubief, Reynolds-averaged modeling of polymer drag reduction in turbulent flows, J. Non-Newton. Fluid Mech. 165 (7–8) (2010) 376–384, http://dx.doi.org/10.1016/j.jnnfm.2010.01.013.

[16] P.A. Durbin, Separated flow computations with the k-epsilon-v-squared model, AIAA J. 33 (4) (1995) 659–664, http://dx.doi.org/10.2514/3.12628.

[17] M. Masoudian, K. Kim, F. Pinho, R. Sureshkumar, A viscoelastic turbulent flow model valid up to the maximum drag reduction limit, J. Non-Newton. Fluid Mech. 202 (2013) 99–111, http://dx.doi.org/10.1016/j.jnnfm.2013.09.007.

[18] M. Masoudian, K. Kim, F. Pinho, R. Sureshkumar, A Reynolds stress model for turbulent flow of homogeneous polymer solutions, Int. J. Heat Fluid Flow 54 (2015) 220–235, http://dx.doi.org/10.1016/j.ijheatfluidflow.2015.05.017.

[19] M. Malin, Turbulent pipe flow of power-law fluids, Int. Commun. Heat Mass Transfer 24 (7) (1997) 977–988, http://dx.doi.org/10.1016/S0735-1933(97)00083-3.

[20] M.R. Malin, Turbulent pipe flow of Herschel-Bulkley fluids, Int. Commun. Heat Mass Transfer (1998) http://dx.doi.org/10.1016/S0735-1933(98)00019-0.

[21] C.K. Lam, K. Bremhorst, A modified form of the k-ϵ model for predicting wall turbulence, J. Fluids Eng. Trans. ASME (1981) http://dx.doi.org/10.1115/1.3240815.

[22] A. Bartosik, Modelling of a turbulent flow using the Herschel-Bulkley rheological model, Chem. Process Eng. - Inz. Chem. Proces. (2006).

[23] A. Bartosik, Application of rheological models in prediction of turbulent slurry flow, Flow Turbul. Combust. (2010) http://dx.doi.org/10.1007/s10494-009-9234-y.

[24] A.A. Gavrilov, V.Y. Rudyak, Reynolds-averaged modeling of turbulent flows of power-law fluids, J. Non-Newton. Fluid Mech. 227 (2016) 45–55, http://dx.doi.org/10.1016/j.jnnfm.2015.11.006.

[25] F.R. Menter, M. Kuntz, R. Langtry, Ten years of industrial experience with the SST turbulence model turbulence heat and mass transfer, in: Turbulence, Heat and Mass Transfer 4, 2003.

[26] B.E. Launder, G.J. Reece, W. Rodi, Progress in the development of a Reynolds-stress turbulence closure, J. Fluid Mech. (1975) http://dx.doi.org/10.1017/S0022112075001814.

[27] D.C. Wilcox, Reassessment of the scale-determining equation for advanced turbulence models, AIAA J. (1988) http://dx.doi.org/10.2514/3.10041.

[28] J. Singh, M. Rudman, H. Blackburn, The effect of yield stress on pipe flow turbulence for generalised newtonian fluids, J. Non-Newton. Fluid Mech. 249 (2017) 53–62, http://dx.doi.org/10.1016/j.jnnfm.2017.09.007.

[29] J. Singh, M. Rudman, H.M. Blackburn, Reynolds number effects in pipe flow turbulence of generalized Newtonian fluids, Phys. Rev. Fluids 3 (9) (2018) 094607, http://dx.doi.org/10.1103/PhysRevFluids.3.094607.

[30] F.R. Menter, Y. Egorov, D. Rusch, Steady and Unsteady Flow Modelling Using the $k-\sqrt{k}L$ Model, 2011, http://dx.doi.org/10.1615/ichmt.2006.turbulheatmasstransf.800.

[31] P.R. Spalart, S.R. Allmaras, J. Reno, One-Equatlon Turbulence Model for Aerodynamic Flows Boeing, Aiaa, 1992, p. 23, http://dx.doi.org/10.2514/6.1992-439.

[32] R.P. Chhabra, J.F. Richardson, Non-Newtonian Flow and Applied Rheology, Elsevier, 2008, p. 536, http://dx.doi.org/10.1016/B978-0-7506-8532-0.X0001-7.

[33] T.C. Papanastasiou, Flows of materials with yield, J. Rheol. 31 (5) (1987) 385–404, http://dx.doi.org/10.1122/1.549926.

[34] F. Gori, A. Boghi, A three dimensional exact equation for the turbulent dissipation rate of Generalised Newtonian Fluids, Int. Commun. Heat Mass Transfer 39 (4) (2012) 477–485, http://dx.doi.org/10.1016/j.icheatmasstransfer.2012.02.010.

[35] L. Eça, F.S. Pereira, G. Vaz, Viscous flow simulations at high Reynolds numbers without wall functions: Is $y^+ \simeq 1$ enough for the near-wall cells? Comput. & Fluids 170 (2018) 157–175, http://dx.doi.org/10.1016/j.compfluid.2018.04.035.

[36] F.R. Menter, Two-equation eddy-viscosity turbulence models for engineering applications, AIAA J. 32 (8) (1994) 1598–1605, http://dx.doi.org/10.2514/3.12149.

[37] G. Vaz, F. Jaouen, M. Hoekstra, Free-surface viscous flow computations: Validation of URANS code FRESCO, in: Proceedings of OMAE2009, Honolulu, Hawaii, USA, 2009, pp. 425–437, http://dx.doi.org/10.1115/OMAE2009-79398.

[38] S. Lovato, S.L. Toxopeus, J.W. Settels, G.H. Keetels, G. Vaz, Code verification of non-Newtonian fluid solvers for single- and two-phase laminar flows, J. Verif. Valid. Uncertain. Quantif. 6 (2) (2021) http://dx.doi.org/10.1115/1.4050131.

[39] C.M. Klaij, C. Vuik, SIMPLE-type preconditioners for cell-centered, colocated finite volume discretization of incompressible Reynolds-averaged Navier-Stokes equations, Internat. J. Numer. Methods Fluids 71 (7) (2013) 830–849, http://dx.doi.org/10.1002/fld.3686.

[40] B. van Leer, Towards the ultimate conservative difference scheme. V. A second-order sequel to Godunov's method, J. Comput. Phys. 32 (1) (1979) 101–136, http://dx.doi.org/10.1016/0021-9991(79)90145-1.

[41] L. Eça, M. Hoekstra, A procedure for the estimation of the numerical uncertainty of CFD calculations based on grid refinement studies, J. Comput. Phys. 262 (2014) 104–130, http://dx.doi.org/10.1016/j.jcp.2014.01.006.

[42] H.R. Anbarlooei, D.O. Cruz, F. Ramos, A.P. Silva Freire, Phenomenological blasius-type friction equation for turbulent power-law fluid flows, Phys. Rev. E 92 (6) (2015) 5–9, http://dx.doi.org/10.1103/PhysRevE.92.063006.

[43] H. Anbarlooei, D. Cruz, F. Ramos, C. Santos, A. Silva Freire, On the connection between Kolmogorov microscales and friction in pipe flows of viscoplastic fluids, Physica D 376–377 (2018) 69–77, http://dx.doi.org/10.1016/j.physd.2017.11.005.

[44] J. Peixinho, C. Nouar, C. Desaubry, B. Théron, Laminar transitional and turbulent flow of yield stress fluid in a pipe, J. Non-Newton. Fluid Mech. 128 (2–3) (2005) 172–184, http://dx.doi.org/10.1016/j.jnnfm.2005.03.008.

[45] B. Güzel, T. Burghelea, I.A. Frigaard, D.M. Martinez, Observation of laminar–turbulent transition of a yield stress fluid in Hagen–Poiseuille flow, J. Fluid Mech. 627 (2009) 97–128, http://dx.doi.org/10.1017/S0022112009005813.

[46] J. Singh, M. Rudman, H.M. Blackburn, A. Chryss, L. Pullum, L.J. Graham, The importance of rheology characterization in predicting turbulent pipe flow of generalized Newtonian fluids, J. Non-Newton. Fluid Mech. 232 (2016) 11–21, http://dx.doi.org/10.1016/j.jnnfm.2016.03.013.

[47] D.C. Wilcox, Turbulence Modeling for CFD (Third Edition), DCW Industries, 2006.

[48] A.B. Metzner, J.C. Reed, Flow of non-newtonian fluids—correlation of the laminar, transition, and turbulent-flow regions, AIChE J. 1 (4) (1955) 434–440, http://dx.doi.org/10.1002/aic.690010409.

[49] L. Eça, M. Hoekstra, The numerical friction line, J. Mar. Sci. Technol. 13 (4) (2008) 328–345, http://dx.doi.org/10.1007/s00773-008-0018-1.

[50] F.S. Pereira, L. Eça, G. Vaz, Verification and validation exercises for the flow around the KVLCC2 tanker at model and full-scale Reynolds numbers, Ocean Eng. 129 (October 2016) (2017) 133–148, http://dx.doi.org/10.1016/j.oceaneng.2016.11.005.

[51] H.R. Anbarlooei, D.O. Cruz, F. Ramos, C.M. Santos, A.P. Silva Freire, Phenomenological friction equation for turbulent flow of Bingham fluids, Phys. Rev. E 96 (2) (2017) 1–6, http://dx.doi.org/10.1103/PhysRevE.96.023107.